Regular Article

Stochastic resonance in a locally excited system of bistable oscillators

M. Gosak[1,a], M. Perc[1], and S. Kralj[1,2]

[1] Departement of Physics, Faculty of Natural Sciences and Mathematics, University of Maribor, Koroška cesta 160, 2000 Maribor, Slovenia

[2] Jožef Stefan Institute, Jamova 39, 1000 Ljubljana, Slovenia

Abstract. Stochastic resonance is studied in a one-dimensional array of overdamped bistable oscillators in the presence of a local subthreshold periodic perturbation. The system can be treated as an ensemble of pseudospins tending to align parallel which are driven dynamically by an external periodic magnetic field. The oscillators are subjected to a dynamic white noise as well as to a static topological disorder. The latter is quantified by the fraction of randomly added long-range connections among ensemble elements. In the low connectivity regime the system displays an optimal global stochastic resonance response if a small-world network is formed. In the mean-field regime we explain strong changes in the dynamic disorder strength provoking a maximal stochastic resonance response via the variation of fraction of long-range connections by taking into account the ferromagnetic-paramagnetic phase transition of the pseudospins. The system size analysis shows only quantitative power-law type changes on increasing number of pseudospins.

1 Introduction

Stochastic resonance is one of the most interesting phenomena that have been studied in the relation to the response of stochastic nonlinear systems driven by weak external periodic forcing. In particular, the response of the system exhibits a resonance-like dependence on the noise intensity. This intriguing and apparently paradoxical phenomenon has led, even after nearly three decades since its discovery, to a general and prolonged interest (for a comprehensive review see [1,2]). Initial works within the context of stochastic resonance have been related to the analysis of the response of a stochastic overdamped bistable system [3]. Afterwards, the mechanism of stochastic resonance has been widely extended to several other situations, whereby the most prominent example is excitable systems (for a comprehensive review see [4]).

A particular interest has been devoted to the understanding of constructive effects of noise in coupled systems. Seminal investigations were focused on the stochastic resonance in coupled nonlinear overdamped oscillators [5–7]. In this context Neiman et al. [8] provided a general theory based on linear response theory, which serves for the explanation of conventional and aperiodic stochastic resonance in ensembles of stochastic resonators. Later on, similar systems served for several other reports about non-trivial effects of noise, such as array-enhanced stochastic resonance [9–12], system size resonance [13] and

diversity-induced resonance [14]. Besides bistable systems, noise-induced phenomena in spatially extended systems have also been extensively studied in several other set-ups (for a comprehensive review see [15]). While in the past the majority of scientific research dealing with the dynamics of spatially extended systems was devoted to the study of regular networks, recently, the focus has been shifting towards ensembles characterized with complex interaction topologies, as constituted by small-world or scale-free networks [16,17]. Such networks appear to be excellent for modelling of interactions among units in complex systems, since many natural, social, and technological systems can be described in terms of complex networks, in which vertices represent interacting units and the edges are the interactions among them. Examples range from ecological networks [18], scientific-collaboration and other social networks [19], to biological networks [20–22].

Notably, the influence of heterogeneous interaction networks on stochastic resonance and other noise-induced phenomena has already attracted considerable attention in the last few years, whereby in general advantages of complex topologies have been emphasized [23,24]. Furthermore, several studies have been devoted to the weakly driven Ising model studied in the context of stochastic resonance [25–29]. It was shown that the system's response could exhibit two maxima just above and below the dynamic phase transition temperature $T_c^{(dyn)}$ [25–27], whereby the phenomenon was explained by means of the time scaling matching condition [26]. Namely, the intrinsic time scale is given by the dominant relaxation time

a e-mail: marko.gosak@uni-mb.si

τ_r of the system of pseudospins. Thus, at the resonance condition, τ_r should match the extrinsic time scale τ_e of the external driving field. Because τ_r diverges at the critical temperature and decreases as the temperature is raised or lowered from $T_c^{(dyn)}$ the presence of double peaks is expected to appear at temperatures where the condition $\tau_r = \tau_e$ is fulfilled. Obviously, stochastic resonance need not be observed only in one-dimensional Ising systems that are characterized with short-range interactions with the first neighbours. In such systems a second order phase transition does not exist and consequently the condition $\tau_r < \tau_e$ might be obeyed for all temperatures. However, it has been shown that the introduction of random long-range connections into such ensembles drives the system towards the mean-field type behaviour and thus the emerged small-world network structure leads to the existence of a paramagnetic-ferromagnetic transition at a finite critical temperature T_c in the thermodynamic limit [30,31]. In the view of that, Hong et al. [27] studied the stochastic resonance phenomenon of a driven Ising model on small-world networks. They revealed that rewiring in a one-dimensional lattice with local interactions leads to double resonance peaks, as reported previously for two- and three-dimensional or globally coupled one-dimensional systems.

A particularly lively study appears to be the application of localized pacemaker activity in diverse natural systems, even though most of the studies thus far were focused on biological systems [32–34]. Due to the recognized importance of pacemakers, their functioning has widely been theoretically investigated in different situations, including networks with complex interaction topologies [35,36]. Recently, studies focusing on stochastic resonance, complex interaction networks and localized driving have emerged, which in general provide evidence that besides an optimal noise intensity, also an optimal network configuration exists, at which the best global outreach of the pacemaker is obtained [37–41].

In this paper, we extend previous studies by examining the stochastic resonance in a system of coupled bistable oscillators that is locally excited by a weak periodic external field. We consider the influence of topological disorder by tuning the fraction of randomly added long-range connections. A non-trivial behaviour is observed in the region where the fraction of added long-range connections gives rise to an interaction network with small-world properties [42,43]. Moreover, we elucidate the increasing noise intensity that assures an optimal collective response of the system as the fraction of added links is increasing by taking into account the ferromagnetic-paramagnetic phase transition of the pseudospins. We also examine the impact of system size on the reported phenomenon, and provide scaling dependencies with respect to the optimal network topology.

The remainder of this paper is organized as follows. In Section 2 the mathematical model is introduced and basic facts about the stochastic resonance and small-world networks are given. In Section 3 we present and discuss the results. In the last section we summarize our observations.

2 Mathematical model and methods

2.1 Stochastic resonance

We consider a system of N coupled bistable overdamped oscillators perturbed by a local periodic external field. The dynamics of this system is governed by the scaled Langevin equations of the form:

$$\frac{\partial x_i}{\partial t} = x_i - x_i^3 + J\sum_j \varepsilon_{ij}(x_j - x_i) + E_i + \sqrt{2D}\xi_i(t). \quad (1)$$

Dynamical variables x_i describe the state of the ith oscillator located at the ith site (vertex of the network), D is the variance of Gaussian noise with zero mean and autocorrelation $\langle \xi_i(t_1)\xi_j(t_2)\rangle = \delta_{ij}\delta_{t_1 t_2}$. The sum runs over all the oscillators and we set $\varepsilon_{ij} = 1$ for coupled oscillators, whilst otherwise $\varepsilon_{ij} = 0$. The coupling strength between any pair of oscillators is determined with the parameter J. The weak external periodic field (i.e. pacemaker)

$$E_i = E_0 \delta_{i_0 i}\cos(\omega t) \quad (2)$$

is introduced locally at the lattice site $i = i_0$ oscillating with the frequency $\omega = 0.01$ and amplitude $E_0 = 0.08$. We note that the frequency and amplitude of the local forcing are chosen such that in the absence of noise ($D = 0$) the pacemaker is subthreshold, meaning it cannot by itself induce transitions between the two stable steady states; not by the oscillator which is directly exposed and neither by any other constitutive unit of the network. Instead, the oscillator directly perturbed by the pacemaker exhibits small-amplitude oscillations around the minimum of its potential with the frequency ω. Notably, by adjusting the forcing closer to the threshold (e.g. by increasing E_0), yet still remaining in the subthreshold regime to satisfy the traditional setup for stochastic resonance, the noise intensity required for the optimal response of the system expectedly becomes lower. Below we will therefore consider D as one of the crucial system parameters, while the role of the coupling strength J will also be examined.

In order to quantify the collective response of the system to the periodic field E_i, we calculate the Fourier coefficients Q_m for the mean field

$$X = \frac{1}{N}\sum_i x_i, \quad (3)$$

where the coefficients are defined as

$$Q = \frac{\omega}{\pi n}\int_0^{2\pi n/\omega} X(t)e^{i\omega t}dt, \quad Q_m = |Q|. \quad (4)$$

Since the spectral power amplification is proportional to the square of the Fourier coefficients, they represent a suitable and commonly used measure for the quantification of SR. Higher values of Q correspond to a greater extent

of the input frequency ω in the output signal. In addition we define also the local Fourier coefficient Q_i as

$$Q'_i = \frac{\omega}{\pi n} \int\limits_{0}^{2\pi n/\omega} x_i(t)e^{i\omega t}dt, \quad Q_i = |Q'_i|, \qquad (5)$$

measuring the quality of the local response to the localized external periodic excitation. In equations (4) and (5) $n = 100$ signifies the number of oscillation periods used for the calculation, after 20 initial periods of the temporal traces were discarded as transients. All integrals were evaluated over time for the above-stated frequency of the pacemaker $\omega = 0.01$. Additionally, all calculations were averaged over 100 realizations in order to diminish statistical fluctuations originating from the stochastic dynamics and from randomness incorporated in interaction network generations.

2.2 Interaction networks

The oscillators are hosted by a linear array having a periodic boundary, i.e. a ring network as depicted in Figure 1. We consider differently disordered interaction networks, which we distinguish by a single scalar parameter p. The quantity p measures the fraction of randomly added long-range links, where $0 \leqslant p \leqslant 1$. More precisely, the limiting cases $p = 0$ and $p = 1$ represent the regular and the fully connected network, respectively [43]. In the former case each unit is connected to its 4 nearest neighbours (the degree of all vertices in the ring network is $k_0 = 4$) and in the latter case the oscillators are globally coupled (the degree of all vertices is $k = N - 1$). Thus, by the generation of different topologically disordered networks we start with a regular ring where each vertex is connected to its four nearest neighbours, as shown in the left panel of Figure 1, and then attempt adding to each vertex $N - 5$ long-range connections, whereby each of them is established with a probability p provided it does not already exist. An illustration of this process is presented in the right panel of Figure 1 for $p = 0.02$. Notably, since the degree heterogeneity of networks generated in this fashion follows roughly a Poissonian distribution (apart from the two limiting cases $p = 0$ and $p = 1$), the particular placing of the external field ($i = i_0$) is not of vital importance (see e.g. [37,39]), and indeed is averaged out over the 100 independent realizations that we consider for each value of p.

In interaction networks as considered here small-world configurations with very specific properties can emerge. Their existence is characterized by a relatively short average path length $L(p)$ [42,43], which tells us how many links on average we need to pass through to travel between any two nodes. A short average path length is otherwise typically associated with random networks. On the other hand, the cliquishness of a typical neighbourhood in small-world networks is large, like in a regular graph. This characteristic is usually quantified using the clustering coefficient $C(p)$ [42]. In order to calculate $L(p)$ one should count the number of links in the shortest path between
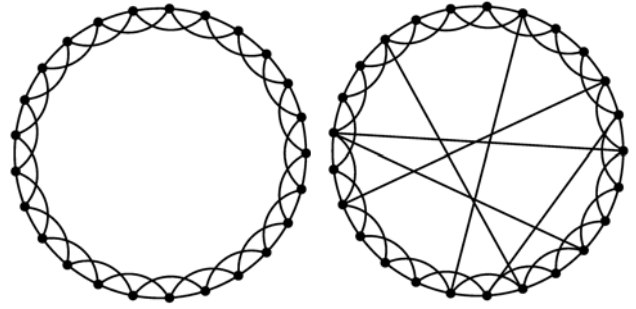

Fig. 1. Examples of considered network topologies. In the left panel a regular ring having $p = 0$ with periodic boundary conditions and vertex degree $k_0 = 4$ is shown, whereas in the right panel the case where long-range links were added with probability $p = 0.02$ (note that six were added) is displayed. For clarity regarding k and p only $N = 25$ vertices are displayed in each panel.

any two vertices, and then average the result over all the pairs. The clustering coefficient is defined as follows. If the node degree (the number of neighbours) of a vertex i is denoted by k_i, there are $k_i(k_i-1)/2$ possible links between these neighbours. One commonly denotes C_i as the fraction of those links that are really present in the graph and $C(p)$ is defined as the average of C_i over all the vertices. In order to determine the onset of an optimal topology for the noise-supported transmission of weak localized signals we introduce the quantity

$$R = \frac{C}{L}, \qquad (6)$$

which has been realized as a suitable indicator for this purpose [37,38], in particular since $R(p)$ has its maximum in the region of p, where the clustering coefficient is quite large, whereas the mean path length is relatively low. Accordingly, a proper ratio between those quantities indicates small-world properties of the network.

3 Results

First, we consider a system of $N = 100$ coupled oscillators where the localized periodic excitation is positioned in the middle (i.e. $i_0 = N/2$) of the array. We focus on the stochastic resonance response of the system as a function of D upon increasing p by means of analysing the transmission of localized rhythmic activity via Q_m and Q_i. On varying p we roughly distinguish between two qualitatively different regimes, to which we refer to as the "low connectivity regime" and the "high connectivity regime". In the first regime the one-dimensional character of the system is pronounced. In the second regime the mean field-type behaviour is observed due to sufficient number of long-range connections. The crossover between the two regimes roughly takes place at $p = p_c \approx 0.03$. Figure 2 features the two-dimensional variation of the global response Q_m upon increasing D and p for both connectivity regimes. In the *low connectivity regime*, $D_{max}(p)$, which denotes the optimal noise intensity at which the best response is observed,
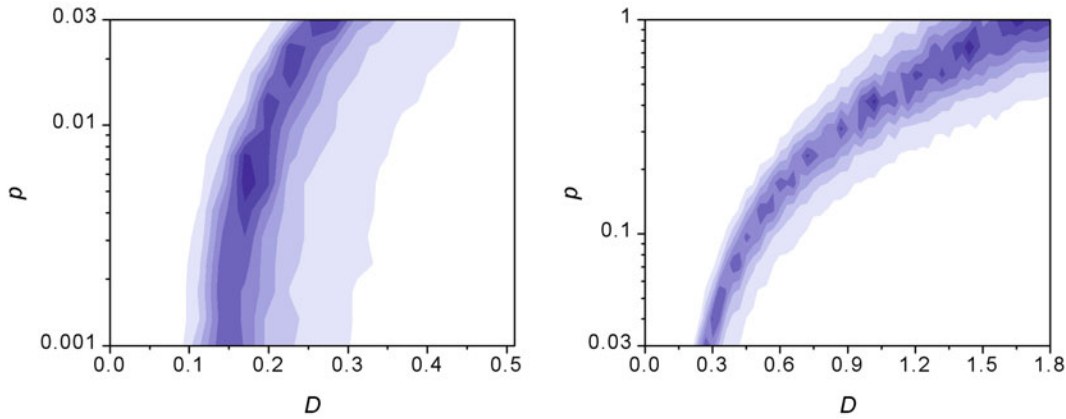
Fig. 2. (Color online) The response of the system quantified via Q_m as a function of the noise intensity D and the fraction of added long-range links p for the low connectivity regime (left panel) and for the high connectivity regime (right panel) (see also main text for details). The color profile is linear, white depicting 0.0 and blue 0.02 values of Q_m. The coupling strength was $J = 0.1$ in both panels.

displays relatively weak changes in dependence on p. On the other hand, in the *high connectivity regime*, $D_{max}(p)$ increases strongly and monotonously upon increasing p. In addition, we observe a rather complex behaviour of the maximal stochastic resonance response Q_m $(D = D_{max})$ as a function of p. In particular, in the *low connectivity* regime we notice a nonmonotonous resonance-like response in dependence on p, whereas in the *high connectivity* region Q_m $(D = D_{max})$ is increasing with increasing values of p. In the following the observed behaviour will be examined in more detail.

3.1 Low connectivity regime

We first focus on the *low connectivity* regime, which extends across the interval $p \in [0, p_c]$. For a constant value of p the $Q_m(D)$ dependence exhibits a resonant outlay due to the existence of an optimal noise intensity, which is typical for the stochastic resonance phenomenon. Figure 3 features the results for different values of p and two different coupling strengths J. Importantly, we can corroborate that there exists an optimal fraction of added long-range links p (blue triangles; $p \approx 0.007$) at which the best collective response Q_m $(D = D_{max})$ is realized. Furthermore, the effect is robust on variations of the coupling strength, except that D_{max} increases with increasing values of J, which will be further addressed in Section 3.2.

In order to gain more insights into the phenomenon, we monitor the mean characteristics of interaction networks for different values of p via the above-introduced quantities; namely the mean shortest path $L(p)$, the clustering coefficient $C(p)$ and their ratio $R(p)$. Results are shown in Figure 4. Upon increasing p the $L(p)$ dependence decreases rather fast already for very small values of p (note the logarithmic scale for p in Fig. 4). On the other hand $C(p)$ begins to decrease considerably only at higher values of p. Consequently, the peak of $R(p)$ occurs at an intermediate value of p ($p = p_{SW} \approx 0.007$), signifying the section, where the clustering is relatively large by comparison with
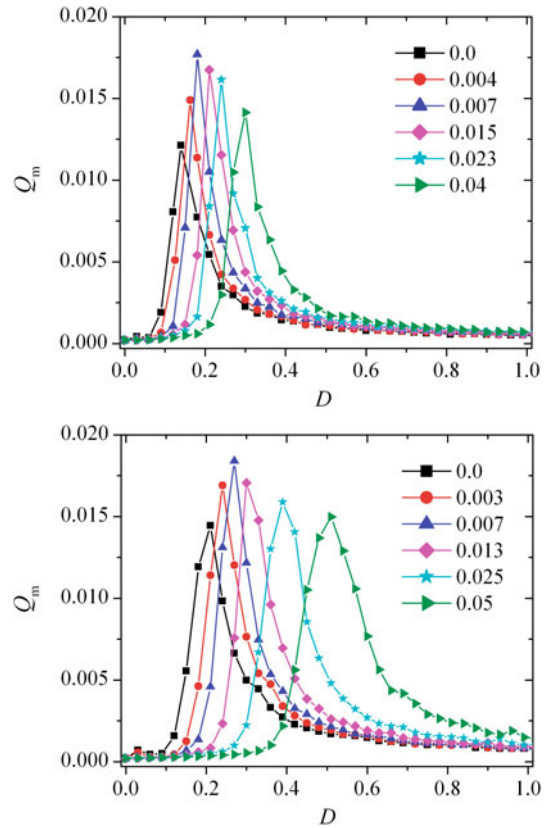

Fig. 3. (Color online) The Fourier coefficient of the mean field Q_m as a function of the noise intensity D for different values of p and for different values of the coupling strength; $J = 0.1$ (upper panel) and $J = 0.2$ (lower panel). Evidently, the optimal network topology is unaffected by the coupling strength, equalling $p = p_{SW} \approx 0.007$, only the noise intensity required for the optimal response increases with increasing values of J.

the average path length. Those are features which signal the emergence of a small-world network topology [37,38]. It can be inferred that this is network configuration enables an optimal transfer of a locally excited perturbation
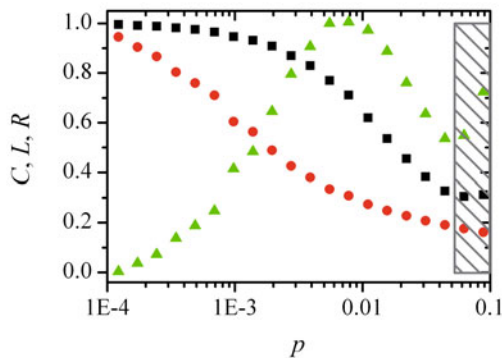
Fig. 4. (Color online) The normalized shortest path (L – red circles) and clustering coefficient (C – black squares), as well as the ratio of the two ($R = C/L$ – green triangles) as a function of p. The peak of R occurs at $p = p_{SW} \approx 0.007$ revealing that a small-world topology is in place. By values of p extending into the grey-hatched region the mean-field effect becomes dominant and thus R is no longer an appropriate measure. Note that R has been rescaled to the unit interval for the purpose of better visualization, but the outlay of the curve has thereby been completely preserved.

into the surrounding area. Namely, the optimal collective response that is observed in Figure 3 for $p = p_{SW} \approx 0.007$ can be ascribed to the emergence of this particular feature of the interaction network, in particular since it emerges by the same value of p where also $R(p)$ has its maximum.

We additionally examine the positional smearing of the locally excited perturbation by calculating the response of individual units Q_i as a function of D for different values of p. Results presented in Figure 5 confirm that at $p = p_{SW}$ the noise-induced outreach of the local perturbation across the whole array is optimal. Clearly, fine-tuning of the network structure via p can optimize the phenomenon of stochastic resonance in an ensemble of locally excited bistable oscillators.

Aiming to further widen the scope of above-reported findings, we analyze the role of varying system size on the reported phenomenon. Figure 6 features Q_i as a function of D for different values of N at the optimal $p = p_{SW}$. Note that the results presented in Figure 4 demonstrate clearly that the optimal topology for the noise-supported transmission of the localized forcing emerges only when the network has properties that are typical for small-worlds. Since the specific value of p warranting the small-world properties depends on N, the optimal $p = p_{SW}$ needs to be adjusted accordingly (see also the left panel of Fig. 7 below). From results presented in Figure 6 it is evident that the optimal response region is always centred on the oscillator that is directly perturbed by the pacemaker. This in turn implies that as the system size increases the maximally attainable Q_m by the optimal values of D and p decreases because the units that are far away from the pacemaker contribute increasingly less to the overall coherence of the system with the external forcing. This can be observed clearly by larger N, where the region of optimal response is extremely narrow, especially if compared

to the overall system response further away from the pacemaker. In comparison, for smaller system sizes the region of optimally coherent response appears wider, which in turn implies higher Q_m. In what follows, we will investigate the outlined dependencies on N quantitatively.

As it was shown that the optimal stochastic resonance response is obtained at $p = p_{SW}$, where the network's $R(p)$ has its maximum and thus exhibits small-world properties (see Fig. 4), we first explore more precisely how p_{SW} varies with the system size. Results in the left panel of Figure 7 reveal that p_{SW} decreases with increasing system size. Notably, the relation is of the form

$$p_{SW} \propto N^{-1}. \tag{7}$$

This relation implies that in the proposed network model [43] the number of long-range links that have to be added in order to attain the optimal network structure does not depend on the system size, whereby of course, the fraction of required long-range connections decreases as N is increased. The observed scaling relation has to be considered by analyzing the role of varying system size, since $p = p_{SW}$ is directly linked to the emergence of the small-world topology at each particular N, as evidenced in Figure 4 for $N = 100$. Subsequently, we are now equipped to proceed with calculating the $Q_m(D)$ dependence for $N = 50$ and $N = 800$, whereby in both cases we take into consideration three characteristic values of p. In particular, we consider the regular network limit ($p = 0$), the value of p matching the optimal p_{SW} from the left panel of Figure 7, and the third value that is higher than p_{SW} but is still located in the *low connectivity regime* for any given N. Results are shown in the middle panel of Figure 7. Evidently, in both cases the optimal response is achieved at $p = p_{SW}$, as already presented in Figure 3 where the system size was $N = 100$, which confirms that the reported phenomenon is qualitatively independent on the system size. Importantly, however, the overall values of Q_m decrease notably as N increases, which reflects the fact that the periodic excitation is applied only to a single oscillator, so that consequently its relative importance deteriorates with increasing N. To quantify this effect more precisely and relevantly, we calculate the degree of stochastic resonance optimisation via the difference in Q_m ($D = D_{max}$) at $p = p_{SW}$ and Q_m ($D = D_{max}$) at $p = 0$ for different system sizes. Results in the right panel of Figure 7 indicate that the absolute difference declines with increasing N. However, this reduction reflects the decrease in the absolute values of Q_m ($D = D_{max}$), whereas importantly, the relative difference between the maxima at $p = p_{SW}$ and $p = 0$ remains practically constant if normalized with it. In particular, the optimization of the resonant response attained by a proper addition of long-range connections is always around 20%, irrespective of the system size.

3.2 High connectivity regime

In the *high connectivity* region oscillators are relatively strongly coupled due to the substantial number of
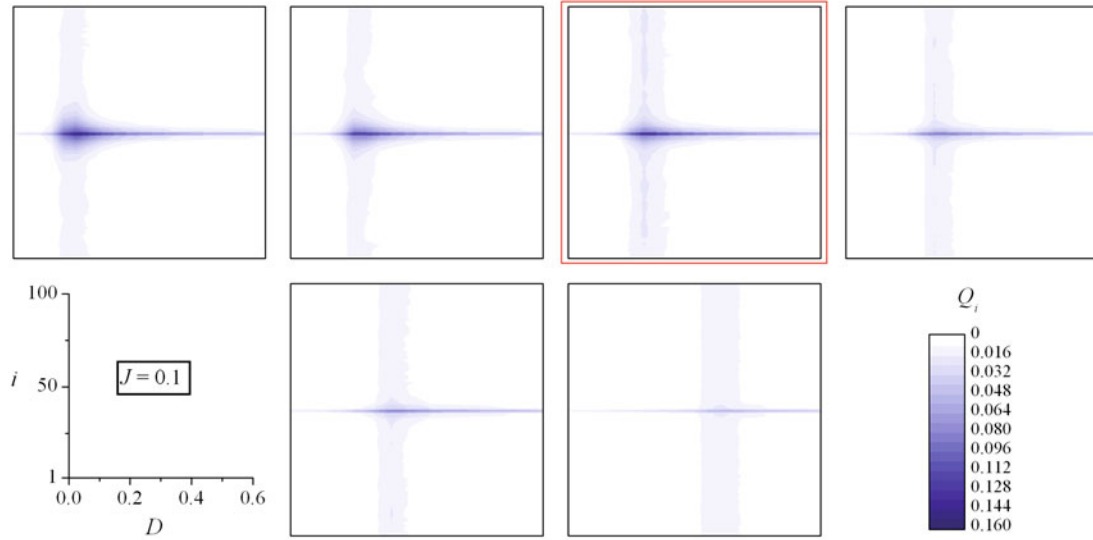
Fig. 5. (Color online) Two-dimensional representation of the response of individual units Q_i. From top left to bottom right p is equal to 0.0, 0.004, 0.007, 0.015, 0.023 and 0.06. Evidently, the weak local perturbation extends at finest across the whole array at $p = p_{SW} \approx 0.007$ (encircled red), where the network has properties that are characteristic of small-worlds. The colour profile is the same in all panels (see bottom right), whereas the content of horizontal and vertical axes is given in the bottom left panel.
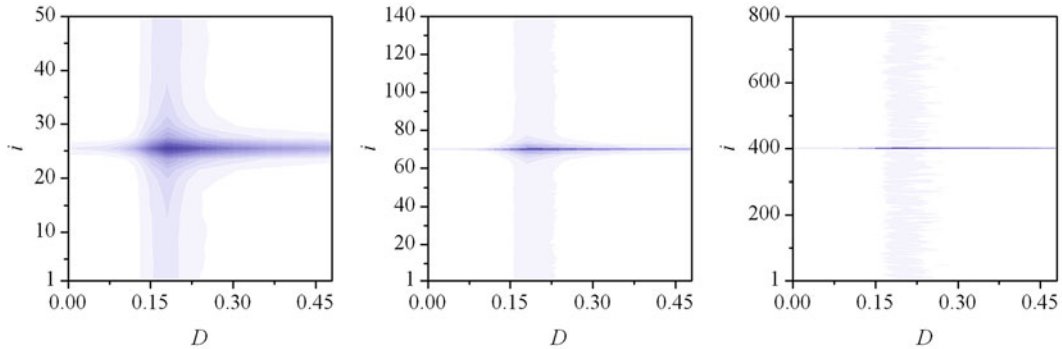

Fig. 6. (Color online) Two-dimensional representation of the response of individual units Q_i for different system sizes at the optimal network configuration $p = p_{SW}$, manifesting in the emergence of the small-world topology. From the left to the right panel N is equal to 50, 140 and 800, while $p = p_{SW}$ is 0.015, 0.006 and 0.0012 (see also the left panel of Fig. 7), respectively. The colour profile is the same as defined in Figure 5 and is identical in all three panels. The coupling strength was $J = 0.1$ for all N.

long-range links connecting them with one another. With increasing values of p the mean field limit is progressively approached and herewith the value of $D_{max}(p)$, where the best correlation between the system's response and the periodic driving is obtained, increases as well, as outlined in the main text pertaining to Figure 2. In this section we focus on the physical reasons behind this finding.

Note that the "interaction part" in equation (1) can be obtained from the minimization of the scaled Hamiltonian

$$H = \sum_i \left(-\frac{1}{2}x_i^2 + \frac{1}{4}x_i^4 \right) + \frac{J}{2} \sum_{i,j} \varepsilon_{ij}(x_i - x_j)^2 - \sum_i x_i E_i$$

$$(8)$$

of a system of pseudospins, the dissipation rate of which is given by $F_{dis} = \sum_i \frac{1}{2} \left(\partial x_i / \partial t \right)^2$. In the thermodynamic limit the thermal noise contribution (see the last term in the right side of Eq. (1)) introduces the temperature T into the system. The 1st (condensation) term in equation (8) enforces $x_i = \pm 1$, the second (coupling) term favours $x_i = x_j$ for $J > 0$ and the last (external field) term tends to align pseudospins along the field direction. Note that the coupling term $\frac{1}{2} \sum_{i,j} \varepsilon_{ij}(x_i - x_j)^2 = -\sum_{i,j} \varepsilon_{ij}x_ix_j + \sum_{i,j} \varepsilon_{ij}x_i^2$ slightly differs from the typical Ising interaction term $-\sum_{i,j} \varepsilon_{ij}x_ix_j$ [44–47]. However, our analysis shows that ordering tendencies of both models are similar as it is shown in Appendix. For that reason the employed analogy with
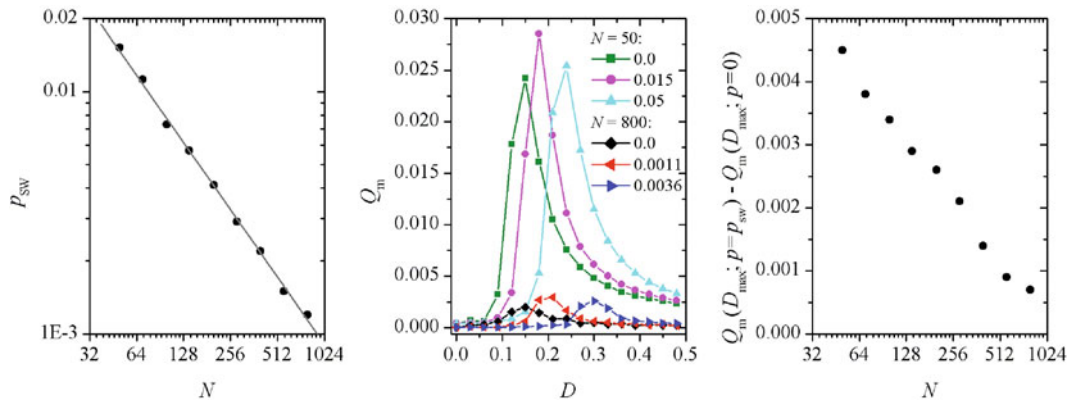
Fig. 7. (Color online) The left panel features the optimal fraction of long-range links p_{SW} in dependence on the system size N. The slope of the solid line is equal to –1, while the dots are numerically obtained values. The middle panel depicts Q_m as a function of the noise intensity D for $N = 50$ and $N = 800$ and for three characteristic values of p. Right panel shows the level of optimization of the stochastic resonance response (see also main text for details) evoked by the optimal network topology in dependence on N. The coupling strength in the middle and right panel was $J = 0.1$.
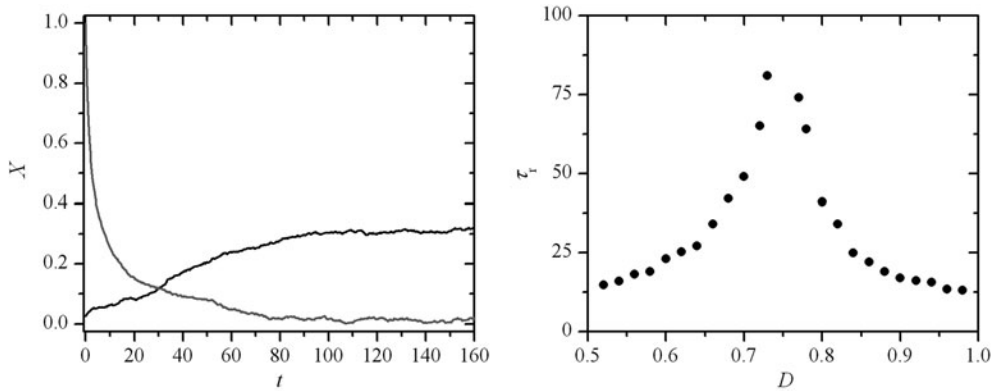

Fig. 8. The left panel features the relaxation of $X(t)$ towards the ferromagnetic ($D = 0.7$, black line) and the paramagnetic ($D = 0.8$, grey line) equilibrium configuration. In the right panel the relaxation time τ_r is depicted versus the noise intensity D. In both panels no external field was applied, $p = 0.1$ and $N = 10\,000$.

the Ising model, on the basis of which we provide an explanation for the observed behaviour, is completely justified.

As it was shown previously [27,28,30,31], the one-dimensional kinetic Ising model exhibits a paramagnetic-ferromagnetic phase transition if long-range interactions are present in the model. This transition is static for $E_i = 0$, taking place at $T = T_c$ (i.e. $D = D_c$). In the presence of the external field E_i, the transition is dynamic and realized at $T = T_c^{(dyn)}$ ($D = D_c^{(dyn)}$). However, for weak enough external fields, it holds $T_c \sim T_c^{(dyn)}$ ($D_c \sim D_c^{(dyn)}$) [27]. The behaviour of our system is revealed in Figure 8, where we show for $p = 0.1$ the relaxations of $X(t)$ towards equilibrium, starting from a nonequilibrium configuration at $t = 0$ for $D > D_c$ (i.e. $T > T_c$) and $D < D_c$ in the absence of the external driving field. In both cases one observes exponential-like relaxation that can be characterized by the relaxation time τ_r, towards paramagnetic and ferromagnetic equilibrium configuration, respectively. In order to evaluate the phenomenon more quantitatively, we calculate the relaxation time τ_r as a function of D.

Results presented in the right panel of Figure 8 clearly indicate the phase transition at $D = D_c$.

The reported phase behaviour of our system described above explains the $D_{max}(p)$ dependence observed in Figure 2, where the role of temperature T in the thermodynamic limit is played by the dynamic noise D. Namely, the phase transition temperature of our system in the thermodynamic limit is approximately determined by the condition (see Appendix A).

$$k_b T_c \approx V_0 + \overline{k}\, J, \tag{9}$$

where k_b stands for the Boltzmann constant, V_0 stands for the typical energy scale of the bistable potential and $\overline{k}$ is the average degree of the network. As already mentioned above, in the presence of an external periodic excitation field the static phase transition at $D = D_c$ (corresponding to $T = T_c$) is replaced by a dynamic phase transition realized at $D = D_c^{(dyn)}$ (corresponding to $T = T_c^{(dyn)}$). Accordingly, equation (9) implies that $D_c^{(dyn)}$ includes a term which is proportional with $\overline{k} \propto p$. In particular, by taking into account that $\overline{k} = k_0[1 + p(N - 1 - k_0)]$ and

$D_c^{(dyn)} \sim D_c$, the relation between phase transition point D_c and the fraction of added long-range connections p can be expressed as follows:

$$D_c \propto V_0 + J k_0[1 + p(N - 1 - k_0)]. \tag{10}$$

Furthermore, due to finite size effects ($N < \infty$) the expected singularity at $D_c^{(dyn)}$ is suppressed. However, the dominant relaxation time τ_r of our system still displays a finite maximum at a noise strength D_c, playing the role of T_c in the limit $N \to \infty$.

The maximal stochastic resonance response is anticipated when the condition

$$\tau_r \approx \tau_e = \frac{2\pi}{\omega} \tag{11}$$

is fulfilled. Note that in the thermodynamic limit a double peak just above and below D_c would be expected. However, within our resolution we observe only a single peak centred roughly at D_c. Nevertheless, since it is known that $D_{max} \propto T_c \propto p+$constant, it is obvious that consequently the greatest response of the system Q_m ($D = D_{max}$) is shifted towards higher values of D as p is increased. Moreover, an analogous reflection also explains the increase in D_{max} as the coupling strength J is increased, which has been observed in Figure 3. Namely, according to equations (9) and (10), it also holds that $D_{max} \propto T_c \propto J$ and hence the optimal response of the system shifts towards higher intensities of dynamical noise in this case as well.

Finally, we verify theoretical findings presented in this section by numerical simulations. In Figure 9 we show values of D_c and D_{max} as a function of p. It can be observed that there is an approximately linear relation between D_c and p, as indicated in equation (10). Furthermore, values of D_c and D_{max} roughly coincides for different values of p, which confirms that the maximal stochastic resonance response is indeed linked with the paramagnetic-ferromagnetic phase transition.

4 Discussion

We have studied the noise-induced dynamics of an ensemble of coupled bistable oscillators that was excited by a local subthreshold periodic external field. Thereby the one-dimensional limit was considered (ring network) and the level of connectivity was altered by introducing a topological disorder p into the system. The limiting cases (i) $p = 0$, and (ii) $p = 1$ correspond to ordered interaction networks, where each oscillator is coupled with (i) its four nearest neighbours, or (ii) with all remaining oscillators, whereas $0 < p < 1$ indicates a certain degree of topological randomness. We have monitored the system's collective response as a function of p and dynamical noise intensity D, whereby we have distinguished between the *low* and the *high connectivity regime*. In the former regime, the optimal noise intensity D_{max}, at which the greatest synchrony between the localized periodic driving and the system's collective response was observed, exhibits
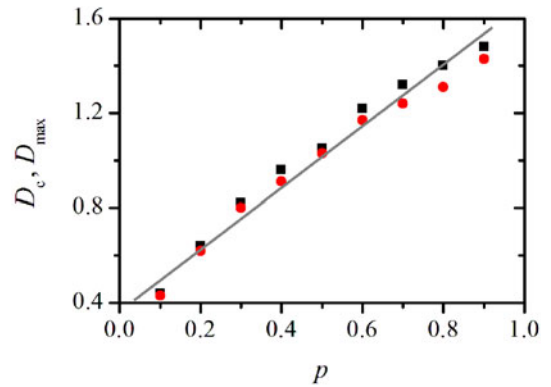

Fig. 9. (Color online) Phase transition point D_c (red circles) and the optimal noise intensity D_{max} (black squares) as a function of p.

a relatively weak dependence on p. Remarkably, however, there exists an optimal fraction of randomly added long-range links p, at which the best outreach of the localized activity was observed, thus indicating also an optimal global response. We have explained the phenomenon by revealing that small-world properties in the interaction network emerge at optimal values of p. We have also analysed the role of varying system size and showed that, on one hand, the best possible global response decreases with increasing system size, but on the other hand, the relative level of optimization via added long-range links is always around 20%, thus leading to the conclusion that the phenomenon is qualitatively independent on the system size. However, as a result of the characteristics of the network, the optimal value of p scales as given in equation (7). In the *high connectivity regime* the mean field effect prevails and here $D_{max}(p)$ monotonously increases with increasing p. We have attributed this behaviour to the transition between the paramagnetic and ferromagnetic phase in the thermodynamic limit, where the system roughly corresponds to the ensemble of pseudospins that are coupled via an Ising-type interaction. Namely, the maximal response is obtained when the time scaling matching condition is fulfilled [26], which is roughly realized at the dynamic phase transition temperature $T_c^{(dyn)}$ (i.e. at the critical noise intensity). Due to the fact that $T_c^{(dyn)}$ increases with the degree of connectivity, we have observed strong increments of $D_{max}(p)$ upon increasing p. It should be noted resemblances between the continuous double well system and a discrete two-state Ising-like systems have already been exploited in the past for the explanation of stochastic resonance related phenomena. While McNamara and Wiesenfeld [48] provided an exhaustive theoretical framework for the understanding of stochastic resonance mechanism in individual two-state systems, Siewert and Schimansky-Geier [49] used this simplification to derive analytical expressions for the signal-to-noise ratio and the spectral power amplification of a chain of coupled two-state elements. Their results have revealed that a ferromagnetic-type coupling gives rise to the resonant response in terms of array-enhanced stochastic resonance.

Our results provide an inside into the functioning of coupled bistable devices which are subjected to weak localized activity and noise. Particular interesting examples are biological neural networks, especially because the understanding of weak signal detection and information propagation is of great importance in the domain of computational neuroscience. It has been observed that in a number of different cortical, thalamic and spinal populations neuronal activity operates in a bistable regime [50–52]. Furthermore, fluctuations of channel gating, synaptic release and of background presynaptic activity introduce intrinsic noise, which can provide benefits to the functioning of neurons [51,53,54]. By revealing that only a few long-range connections are needed to enhance the outreach of localized rhythmic activity, we provide some interesting aspects to the subject, despite the fact that the employed network model is very simple. It is worth to mention that in typical neural architectures neurons are mostly connected with their neighbors, but also with some long-range links, which enable a more efficient information transfer [55]. Bistability is also exhibited in mathematical models of social processes, such as opinion formation models [56], whose structure bears many similarities with the Ising model. The options of individuals are considered as binary variables, which correspond for example to the existence of two political parties. The constructive roles of noise [57] and diversity [58] have already been studied in opinion formation models, as well as the role of small-world topology [59]. Our findings might provide some novel insights to this issue, whereby in contrast to previous studies, the periodic excitation signifying the so called fashion wave influences only one individual.

Appendix A: Critical behaviour of the coupling term

In the Appendix we derive critical behaviour of the model using the standard mean field approximation approach. In the absence of an external field the interaction energy is given by

$$H = V_0 \sum_i \left(-\frac{x_i^2}{2} + \frac{x_i^4}{4} \right) + \frac{J}{2} \sum_{i,j} \varepsilon_{ij}(x_i - x_j)^2, \quad (A.1)$$

where V_0 stands for the typical energy scale of the first term in (A.1). The corresponding free energy reads $F = H - TS$, where S stands for the entropy of the system. Let us assume that in a given configuration of N pseudospins N_+ are in the state $x_i = 1$ and N_- in the state $x_i = -1$. In the limit of large number N the entropy can be approximately (neglecting correlations among pseudospins) expressed as [60]

$$S \approx k_b \ln \left(\frac{N!}{N_+!N_-!} \right) \approx -k_b N \left(c_+ \ln c_+ + c_- \ln c_- \right), \quad (A.2)$$

where $c_\pm = N_\pm/N$. We next assume that pseudospins feel an average surrounding and the coupling term in equation (A.1) is rewritten as

$$H_c \approx \sum_{i,j} \frac{J}{2} \varepsilon_{ij} \left(x_i - \bar{x}\right)^2 \approx \frac{J}{2}\bar{k}$$
$$\times \left[N_+ \left(1 - \bar{x}\right)^2 + N_- \left(1 + \bar{x}\right)^2 \right], \quad (A.3)$$

where $\bar{k}$ stands for the average number of neighbours within the network and $\bar{x}$ stands for an average value of x_i. Taking into account $\bar{x} = c_+ - c_-$ one can express the average free energy per lattice site $\bar{f} = \bar{F}/N$ as

$$\bar{f} \approx V_0 \left(-\frac{\bar{x}^2}{2} + \frac{\bar{x}^4}{4} \right) + \frac{J}{2}\bar{k} \left(1 - \bar{x}^2\right) + \frac{k_b T}{2} \Bigg[(1 + \bar{x})$$
$$\times \ln \left(\frac{1 + \bar{x}}{2} \right) + (1 - \bar{x}) \ln \left(\frac{1 - \bar{x}}{2} \right) \Bigg]. \quad (A.4)$$

The equilibrium value of $\bar{x}$ is obtained by minimizing $\bar{f}$ with respect to $\bar{x}$. The system exhibits the 2nd order phase transition at the critical temperature given by

$$T_c = \frac{V_0 + \bar{k}J}{k_b}. \quad (A.5)$$

The critical condition of the original Ising model is reproduced by setting $V_0 = 0$. Note that T_c is proportional to $\bar{k}$ in the limit $\bar{k}J/V_0 \gg 1$.

References

1. L. Gammaitoni, P. Hänggi, P. Jung, F. Marchesoni, Rev. Mod. Phys. **70**, 223 (1998)
2. T. Wellens, V. Shatokhin, A. Buchleitner, Rep. Prog. Phys. **67**, 45 (2004)
3. R. Benzi, A. Sutera, A. Vulpiani, J. Phys. **14**, L453 (1981)
4. B. Lindner, J. García-Ojalvo, A. Neiman, L. Schimansky-Geier, Phys. Rep. **392**, 321 (2004)
5. P. Jung, U. Behn, E. Pantazelou, F. Moss, Phys. Rev. A **46**, R1709 (1992)
6. H. Gang, H. Haken, X. Fagen, Phys. Rev. Lett. **77**, 1925 (1996)
7. M. Morillo, J. Gómez-Ordóñez, J.M. Casado, J. Casado-Pascual, D. Cubero, Eur. Phys. J. B **69**, 59 (2009)
8. A. Neiman, L. Schimansky-Geier, F. Moss, Phys. Rev. E **56**, 12R (1997)
9. J.F. Lindner, B.K. Meadows, W.L. Ditto, M.E. Inchiosa, A.R. Bulsara, Phys. Rev. Lett. **75**, 3 (1995)
10. F. Duan, F. Chapeau-Blondeau, D. Abbott, J. Stat. Mech. **08**, P08017 (2009)
11. J.F. Lindner, B.K. Meadows, W.L. Ditto, M.E. Inchiosa, A.R. Bulsara, Phys. Rev. E **53**, 2081 (1996)
12. F. Marchesoni, L. Gammaitoni, A.R. Bulsara, Phys. Rev. Lett. **76**, 2609 (1996)
13. A. Pikovsky, A. Zaikin, M.A. de la Casa, Phys. Rev. Lett. **88**, 050601 (2002)
14. C.J. Tessone, C.R. Mirasso, R. Toral, J.D. Gunton, Phys. Rev. Lett. **97**, 194101 (2006)

15. F. Sagués, J.M. Sancho, J. García-Ojalvo, Rev. Mod. Phys. **79**, 829 (2007)
16. M.E.J. Newman, A.-L. Barabási, D.J. Watts, *The Structure and Dynamics of Networks* (Princeton University Press, Princeton, 2006)
17. R. Albert, A.-L. Barabási, Rev. Mod. Phys. **74**, 47 (2002)
18. R.J. Williams, E.L. Berlow, J.A. Dunne, A.-L. Barabási, N.D. Martinez, Proc. Natl. Acad. Sci. USA **99**, 12913 (2002)
19. M.E.J. Newman, Proc. Natl. Acad. Sci. USA **98**, 404 (2001)
20. A.-L. Barabási, Z.N. Oltvai, Nat. Rev. Genetics **5**, 101 (2004)
21. O. Sporns, D.R. Chialvo, M. Kaiser, C.C. Hilgetag, Trends Cogn. Sci. **8**, 418 (2004)
22. C. Zhou, L. Zemanova, G. Zamora, C.C. Hilgetag, J. Kurths, Phys. Rev. Lett. **97**, 238103 (2006)
23. Z. Gao, B. Hu, G. Hu, Phys. Rev. E **65**, 016209 (2001)
24. J.A. Acebrón, S. Lozano, A. Arenas, Phys. Rev. Lett. **99**, 128701 (2007)
25. K. Leung, Z. Néda, Phys. Rev. E **59**, 2730 (1999)
26. B.J. Kim, P. Minnhagen, H.J. Kim, M.Y. Choi, G.S. Jeon, Europhys. Lett. **56**, 333 (2001)
27. H. Hong, B.J. Kim, M.Y. Choi, Phys. Rev. E **66**, 011107 (2002)
28. C.P. Herrero, Phys. Rev. E **65**, 066110 (2002)
29. A. Krawiecki, Eur. Phys. J. B **69**, 81 (2009)
30. A. Barrat, M. Weigt, Eur. Phys. J. B **13**, 547 (2000)
31. A. Pękalski, Phys. Rev. E **64**, 057104 (2001)
32. Y. Nagai, H. González, A. Shrier, L. Glass, Phys. Rev. Lett. **84**, 4248 (2000)
33. R.E. Haddock, C.E. Hill, J. Physiol **566**, 645 (2005)
34. M. Gosak, M. Marhl, M. Perc, Physica D **238**, 506 (2009)
35. H. Kori, A.S. Mikhailov, Phys. Rev. Lett. **93**, 254101 (2004)
36. A.J. Steele, M. Tinsley, K. Showalter, Chaos **16**, 015110 (2006)
37. M. Perc, Phys. Rev. E **76**, 066203 (2007)
38. M. Perc, M. Gosak, New J. Phys. **10**, 053008 (2008)
39. M. Perc, Phys. Rev. E **78**, 036105 (2008)
40. M. Gosak, D. Korošak, M. Marhl, Phys. Rev. E **81**, 014101 (2010)
41. M. Gosak, D. Korošak, M. Marhl, New J. Phys. **13**, 013012 (2011)
42. D.J. Watts, S.H. Strogatz, Nature **393**, 440 (1998)
43. M.E.J. Newman, D.J. Watts, Phys. Lett. A **263**, 341 (1999)
44. N. Menyhárd, G. Ódor, J. Phys. A **29**, 7739 (1995)
45. N. Menyhárd, G. Ódor, J. Phys. A **28**, 4505 (1995)
46. G. Ódor, J. Stat. Mech. L11002 (2006)
47. G. Ódor, Rev. Mod. Phys. **76**, 663 (2004)
48. B. McNamara, K. Wiesenfeld, Phys. Rev. A **39**, 4854 (1989)
49. U. Siewert, L. Schimansky-Geier, Phys. Rev. E **58**, 2843 (1998)
50. A. Longtin, A. Bulsara, D. Pierson, F. Moss, Biol. Cybern. **70**, 569 (1994)
51. A. Zaikin, J. García-Ojalvo, R. Báscones, E. Ullner, J. Kurths, Phys. Rev. Lett. **90**, 030601 (2003)
52. C. Monteiro, D. Lima, V. Galhardo, Neurosci. Lett. **398**, 258 (2006)
53. B. Lindner, L. Schimansky-Geier, Phys. Rev. E **61**, 6103 (2000)
54. J.M. Fellous, M. Rudolph, A. Destexhe, T.J. Sejnowski, Neurosci. **122**, 811 (2003)
55. G. Buzsáki, C. Geisler, D.A. Henze, X.-J. Wang, Trends Neurosci. **27**, 186 (2004)
56. W. Weidlich, Phys. Rep. **204**, 1 (1991)
57. P. Babinec, Phys. Lett. A **225**, 179 (1997)
58. C.J. Tessone, R. Toral, Eur. Phys. J. B **71**, 549 (2009)
59. M. Kuperman, D. Zanette, Eur. Phys. J. B **26**, 387 (2002)
60. P.M. Chaikin, T.C. Lubensky, *Principles of condensed matter physics* (Cambridge University Press, Cambridge, 1995)